http://dx.doi.org/10.21577/0103-5053.20170117

J. Braz. Chem. Soc., Vol. 29, No. 1, 88-98, 2018.
Printed in Brazil - ©2018 Sociedade Brasileira de Química

Article

Heteropoly Tungstate Supported on Metal Oxide Catalysts for Liquid Phase Oxidation of Benzyl Alcohol with Hydrogen Peroxide

Han Xiaoxiang,,[a] Kuang Yingying,[a] Xiong Chunhua,[a] Tang Xiujuan,[b] Chen Qing,[a] Wang Kuiwu,[a] Hung Chin-Te,[c] Liu Li-Li[c] and Liu Shang-Bin*,[c]*

[a]*Department of Applied Chemistry and* [b]*College of Environmental Science and Engineering, Zhejiang Gongshang University, 310018 Hangzhou, China*

[c]*Institute of Atom and Molecular Sciences, Academic Sinica, 10617 Taipei, Taiwan*

A series of metal oxide supported tungstophosphoric acid catalysts were prepared by impregnation. The physicochemical and acidic properties of these materials were characterized by a variety of different analytical and spectroscopic techniques, namely Fourier transform infrared spectroscopy (FTIR), X-ray diffraction (XRD), Brunauer-Emmett-Teller (BET) method, and nuclear magnetic resonance (NMR), and exploited as heterogeneous catalysts for selective oxidation of benzyl alcohol (BzOH) with hydrogen peroxide (H_2O_2). Among them, 20 wt.% $H_3PW_{12}O_{40}/CeO_2$ catalyst exhibited the best oxidative activity. Further process optimization by response surface methodology (RSM) based on the Box-Behnken design model resulted in a benzyl alcohol conversion of 95.2% and a benzaldehyde yield of 94.2% with 98.9% selectivity, in good agreement with the experimental results. Kinetic studies based on an irreversible parallel reaction model led to an activation energy (E_a) of 44.73 kJ mol^{-1}.

Keywords: ceria, heteropolyacid, oxidation, reaction engineering, process optimization

Introduction

Aldehydes and ketones, which are important chemical intermediates, play critical roles in chemical industries and have been extensively used in drugs, additives and spices industries.[1-4] These carbonyl compounds are normally produced by selective catalytic oxidation, which has been widely used in clean production of chemicals.[5-9] One of the major concerns for oxidation reaction is product selectivity, a challenge arising from the fact that most products are thermodynamically unstable. Typically, transition-metal salts or complexes, especially precious metals, are commonly used as homogeneous or heterogeneous catalysts for oxidation reactions.[10] However, excessive consumptions of these metal catalysts are not only cost-ineffective but also created a great number of heavy-metal wastes. Thus, the development of green, cheap, and efficient catalyst systems is a demanding task. In this context, the research and development (R&D) of eco-friendly catalysts such as polyoxometalates (POMs) catalysts have received considerable attention. Among them, heteropolyacids (HPAs) with Keggin-type structure, which possess unique features such as low volatility, non-corrosive, non-toxic, strong Brønsted acidic strength, and excellent redox properties, have been extensively studied and utilized as solid acid catalyst for heterogeneous reactions.[11-14] Nonetheless, owing to their high solubility in polar solvents, HPA-based catalyst systems are drawback by their difficulty in catalyst separation and recycling. As such, modified HPA catalysts, particularly those that may be easily prepared using a feasible support, open up a wide new possibilities to unravel the aforementioned problems.[15-18] As such, while metal or heteroatom substituted HPAs with an exotic variety of structures and compositions have been widely utilized in heterogeneous and/or homogeneous reactions,[19-21] it is highly desirable to support them on a porous solid substrate with unique catalytic and porous properties. The high surface area available for the supported HPA catalyst was found to promote diffusion of reactants/products and dispersion of active sites to warren high catalytic activity with improved product quality, reduced production costs as well as a prolonged catalyst life due to improved robustness, recovery, and recyclability.[22-26]

In the present work, we aim at the preparation of ceria (CeO_2) supported tungstophosphoric acid ($H_3PW_{12}O_{40}$;

*e-mail: hxx74@126.com; sbliu@sinica.edu.tw

HPW) catalysts by means of incipient wetness impregnation method. The physicochemical properties of these HPW/CeO_2 composites were characterized by a variety of different techniques, *viz.* Fourier transform infrared spectroscopy (FTIR), X-ray diffraction (XRD), Brunauer-Emmett-Teller (BET) method, and solid-state ^{31}P magic-angle spinning (MAS) nuclear magnetic resonance (NMR). The catalytic performances of these supported catalysts were assessed by oxidation of benzyl alcohol (BzOH) with hydrogen peroxide (H_2O_2). The corresponding reaction process and product optimization were studied by response surface methodology (RSM) and a kinetic model was also established for the alcohol oxidation reaction under optimized conditions. The satisfying catalytic activity observed for the supported HPW/CeO_2 catalysts may be attributed to the unique redox properties and oxygen storage capacity (OSC)[27-30] as well as the desirable strong acidity and capability of activating oxidant during oxidation of alcohol.[31,32] By comparison, other POMs-based catalysts such as $PMo_{11}Co$ showed lower catalytic activity with only ca. 51% benzaldehyde yield during oxidation of BzOH with H_2O_2.[21]

Experimental

Materials and catalyst preparation

Analytical grade ceria (CeO_2), titania (TiO_2), zirconia (ZrO_2), benzyl alcohol ($C_6H_5CH_2OH$; BzOH), hydrogen peroxide (H_2O_2, 30%), tungstophosphoric acid ($H_3PW_{12}O_{40}$; HPW), and other chemicals were purchased commercially and used without further purification unless otherwise specified.

All supported HPW/CeO_2 catalysts were synthesized using an incipient wetness impregnation method with varied HPW to total weight of HPW and CeO_2 ratios. The supported catalyst samples so prepared are hereafter denoted as xHPW/CeO_2, where x = 15-25 wt.%. For example, the 20HPW/CeO_2 catalyst was prepared by impregnating ca. 4.0 g of ceria support with a 3 mL aqueous solution of HPW (115.8 mmol L^{-1}) for 12 h, followed by first drying overnight at 120 °C, then calcined at 250 °C in static air for 4 h. Similar procedures were used to prepare other supported catalysts.

Catalyst characterization

FTIR measurements were performed at room temperature on a Bruker IFS28 spectrometer. Each spectrum was accumulated by 32 scans between the range of 400-4000 cm^{-1} at a resolution of 1 cm^{-1}. X-ray diffraction (XRD) studies were conducted on a Bruker D8 ADVANCE diffractometer equipped with a Ni-filtered Cu Kα radiation operated at 40 kV and 20 mA. The room temperature XRD patterns were recorded within a 2θ angle range of 5-80° at a scanning rate of 10° min^{-1}. N_2 adsorption/desorption isotherm measurements were performed on a Quantachrome NOVA 1000e physisorption analyzer operating at −196 °C. The acid properties of various catalyst samples were characterized by means of a ^{31}P-TMPO MAS NMR approach, namely solid-state ^{31}P magic-angle spinning (MAS) NMR of adsorbed trimethylphosphine oxide (TMPO) probe molecule.[33-37] All ^{31}P spectra of adsorbed TMPO on various solid acid catalyst samples were recorded at a Larmor frequency of 202.46 MHz using a single-pulse sequence under the conditions: pulse-width (π/6), 1.5 μs; recycle delay, 10.0 s; sample spinning rate, 12 kHz. The ^{31}P chemical shifts (δ^{31}P) were referred to that of 85% H_3PO_4 aqueous solution. Detailed sample preparing procedures involved for acidity characterization using the ^{31}P-TMPO MAS NMR approach can be found elsewhere.[33,34,39]

Catalytic reaction

The catalytic activities of various catalysts were assessed by oxidation of benzyl alcohol (BzOH) with hydrogen peroxide (H_2O_2). The reactions were conducted in a reactor consisting of a three-necked flask (100 mL) and a condenser. Typically, equal molar amount (0.05 M) of BzOH and H_2O_2 were introduced to the catalyst in the reactor, the mixture was stirred at a desired reaction temperature for a given period of time. Upon completion of reaction, the reaction mixture was separated by extraction with ethyl acetate. A gas chromatography (GC; Agilent 7890B) analyzer equipped with a flame ionization detector (FID) and an HP-5 capillary column was used to analyze the compositions of reaction mixture in conjunction with authentic samples.

Experimental design and mathematical model

On the basis of single factor experiments, response surface methodology (RSM) study assisted by a Design-Expert 6.0.5 software (Stat-Ease, USA) was employed to optimize the reaction parameters of BzOH oxidation reaction over the 20HPW/CeO_2 catalyst, which was found to show best catalytic performance (*vide infra*). A three-level, four-variable Box-Behnken design (BBD) model was adopted to investigate the effects of four independent process variables, namely amount of catalyst (x_1), BzOH/H_2O_2 molar ratio (x_2), reaction time (x_3), and

amount of water (x_4), on primary product yield, that is, benzaldehyde (BzH).

All factors in the experiment were coded into three levels, namely −1, 0, and +1 as shown in Table 1. A total of 29 experimental sets, including 24 factorial points and 5 central points, were adopted for the experimental design. Accordingly, the predicted response (product yield; Y) may be expressed as:

$$Y = \beta_0 + \sum_{i=1}^{4} \beta_i x_i + \sum_{i=1}^{4} \beta_{ii} x_i^2 + \sum_{i<j}^{4} \beta_{ij} x_i x_j \quad (1)$$

where x_i and x_j (i, j = 1-4) represents the coded levels of various independent variables, and β_0, β_i, β_{ii}, and β_{ij} are regression coefficients representing the offset, linear, quadratic, and interactive terms of the variables, respectively.

Table 1. List of symbols for various experimental variables and corresponding coded levels and ranges adopted in the experimental design

Variable	Symbol	Range and level		
		−1	0	+1
Amount of catalyst / g	x_1	0.7	0.8	0.9
Alcohol/hydrogen peroxide / (mol mol^{-1})	x_2	1:1	1:2	1:3
Reaction time / h	x_3	3	4	5
Amount of water / mL	x_4	15	20	25

Kinetic study

The kinetic parameters associated with conversion of BzOH were also monitored for the 20HPW/CeO_2 catalyst. By varying the reaction times and temperatures the reaction rate (r) for oxidation of BzOH with H_2O_2 to BzH may be derived by the equation:

$$r = -\frac{dC_A}{dt} = k' C_A^{\alpha} C_B^{\beta} \quad (2)$$

where C_A and C_B represents the concentration of BzOH and H_2O_2, respectively, k' is the rate constant, and α and β denote the reaction order of BzOH and H_2O_2, respectively. By taking the natural log of both sides, the above equation may further be expressed as:

$$\ln r = \ln k + \alpha \ln C_A \quad (3)$$

where $k = k' C_B^{\beta}$ denotes the modified rate constant. By measuring the k values at various temperatures, the activation energy (E_a) could be derived from the Arrhenius equation:

$$\ln k = \ln k_0 - \frac{E_a}{R}\frac{1}{T} \quad (4)$$

where k_0 represents the pre-exponential factor, R is the gas constant, and T is the reaction temperature.

Results and Discussion

Characterization of catalysts

FTIR spectroscopy is employed to elucidate chemical compositions and local configurations of various catalyst samples. The FTIR spectra of CeO_2, HPW and HPW/CeO_2 with varied HPW loadings are shown in Figure 1. Similar to the pristine HPW (Figure 1a), the supported HPW/CeO_2 catalysts showed multiple absorption bands between 4000 and 400 cm^{-1} (Figures 1c-1e). The broad overlapping absorption bands centering at ca. 3435 cm^{-1} may be ascribed to stretching vibrations of O–H. The signals at 1080, 983, 889, and 804 cm^{-1}, which may be attributed to asymmetric stretching vibrations of P–O, terminal vibration of W=O, corner-sharing W–O_b–W, and edge-sharing W–Oc–W bonds, respectively, are characteristic bands anticipated for the Keggin-type unit of the $PW_{12}O_{40}^{3-}$ (PW) polyanions.[39] Clearly, these characteristic peaks are absent in the FTIR spectrum observed for the pure CeO_2 support (Figure 1b). Moreover, the presence of weaker absorption bands at ca. 598 and 516 cm^{-1} may be attributed to symmetric vibrations of O–P–O and W–O–W, respectively.[33] Regardless of minor variations in intensities of characteristic bands responsible for the PW polyanions, their presence in all supported HPW/CeO_2 catalysts confirm that Keggin structure remains intact upon supporting varied

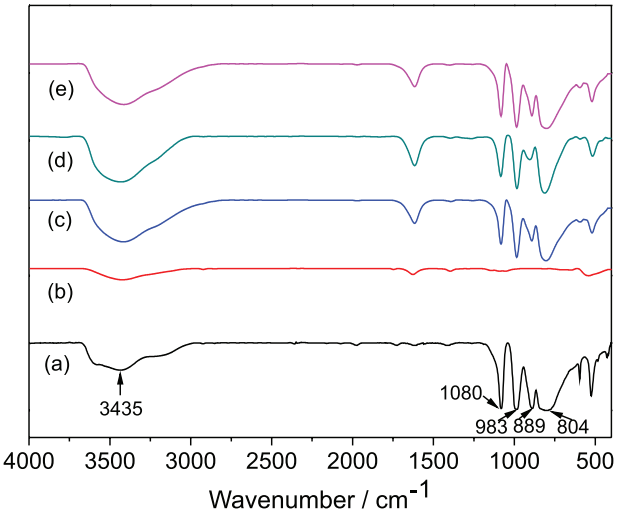

Figure 1. FTIR spectra of (a) the pristine HPW; (b) pure CeO_2; (c) 15HPW/CeO_2; (d) 20HPW/CeO_2; and (e) 25HPW/CeO_2.

amounts of HPW onto the CeO_2 support.

The crystalline structures of the pure CeO_2, pristine HPW, and various supported HPW/CeO_2 composites with varied HPW loadings were examined by XRD, as shown in Figure 2. The CeO_2 support exhibited XRD profile with well-defined diffraction peaks at 2θ angles of 28.5, 33.4, 46.6, 56.7, 58.0, 69.2, 76.2, and 78.9° (Figure 2a), corresponding to the crystalline lattice planes of (111), (200), (220), (311), (222), (400), (331), and (420), respectively. The above diffraction peaks observed for the as-prepared CeO_2 are in excellent agreement with the face center cubic (fcc) phase structure of ceria (JCPDS Card No. 34-394), as expected. On the other hand, the XRD profile of pristine HPW showed characteristic diffraction pattern anticipated for the PW Keggin unit with main peaks at 10.3, 25.3, and 34.6° (Figure 2b).[26,39] However, these characteristic features were invisible in various supported xHPW/CeO_2 (x = 15, 20, and 25 wt.%) composite materials (Figures 2c-2e). Rather, the XRD profile observed for these supported catalysts were nearly identical with that observed for the as-prepared CeO_2 (Figure 2a). The above results suggested that the incorporated HPW are well-dispersed on the surfaces of the CeO_2 support. Together with the results obtained from FTIR spectroscopy, it is indicative that HPWs are successfully incorporated and homogeneously dispersed on the CeO_2 support.

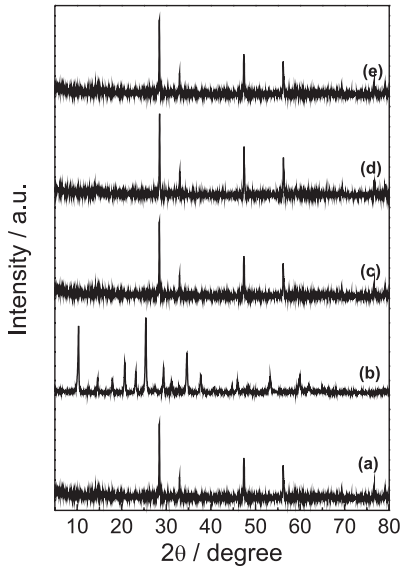

Figure 2. XRD patterns of (a) CeO_2; (b) HPW; (c) 15HPW/CeO_2; (d) 20HPW/CeO_2; and (e) 25HPW/CeO_2.

Additional physisorption studies by N_2 adsorption/desorption isotherm measurements have also been made (not shown). Accordingly, the pristine HPW and the pure CeO_2 samples gave rise to a BET surface area of 6.8 and 26.0 $m^2 g^{-1}$, respectively. However, a somewhat anticipated BET surface area of 11.0, 8.1, and 7.5 $m^2 g^{-1}$ was observed for the 15HPW/CeO_2, 20HPW/CeO_2, and 25HPW/CeO_2 catalysts, respectively. The consistent decrease in surface area with increasing HPW loading observed for the supported catalysts provides additional support to the above FTIR and XRD results to verify that the incorporated HPW was indeed nicely dispersed in the porous CeO_2 support.[40]

The acid properties of various samples were monitored by solid-state ^{31}P MAS NMR using TMPO as probe molecule, which has been shown to be a powerful and reliable technique for acidity characterization.[34,35] Such ^{31}P-TMPO NMR approach relies on the adsorption of a basic probe molecule TMPO onto the acid catalyst. Then the catalyst shows a desirable NMR-sensitive nuclei (i.e., ^{31}P) with a broad range chemical shift (denoted as $\delta^{31}P$). As a result, the probe molecule tends to interact with the available Brønsted acidic protons (H^+) site in the acid catalyst to form $TMPOH^+$ complexes with varied values of $\delta^{31}P$. It has been shown that detailed acid features such as acid types, concentration, distribution, and strength of acid catalysts may readily be determined by means of the ^{31}P-TMPO NMR approach.[34,35] This is made possible by the fact that a linear correlation between the observed $\delta^{31}P$ and acidic strength may readily be inferred.[34-38] Moreover, the acid types and concentration may readily be determined by chemical shift assignment and spectral deconvolution of the observed ^{31}P spectrum. Accordingly, the ^{31}P NMR spectra of TMPO adsorbed on various catalysts are depicted in Figure 3. The spectrum observed for TMPO-adsorbed on pure CeO_2 revealed broad overlapping signals spanning between $\delta^{31}P$ of ca. 35-55 ppm. The ^{31}P resonance centering at ca. 50 ppm should be due to physisorbed TMPO, whereas those centering at ca. 42 and 36 ppm may be attributed to bulk and mobile TMPO, respectively. As for TMPO adsorbed on the pristine TPA, broad resonances centering at three distinct regions with $\delta^{31}P$ of –10 to –15, 55 to 75, and 80 to 95 ppm were observed (Figure 3e), which may be ascribed due to PW Keggin unit, $(TMPO)_nH^+$ adducts ($n > 1.0$), and $TMPOH^+$ complexes, respectively.[34,39] It is noteworthy that the catalyst showed superacidity which exceeds the threshold acidic strength for superacidity (86 ppm).[34-37,39] So the pristine HPW and supported HPW/CeO_2 possess superacidity. Unlike the pristine HPW, an additional peak at ca. 66 ppm was observed for all supported HPW/CeO_2 catalysts (Figures 3b-3d), indicating the presence of Lewis acidity arising from Ce metal centers.[34,35] Similar phenomenon was also found for HPW incorporated on other metal oxide supports such as ZrO_2 and TiO_2, as illustrated in Figure 4. Moreover, it is indicative that the overall strength of acid sites (particularly those with $\delta^{31}P > 80$ ppm) of the supported HPW/CeO_2 catalysts follow the ascending trend: 15HPW/CeO_2 < 20HPW/CeO_2 < 25HPW/CeO_2. Thus, it is

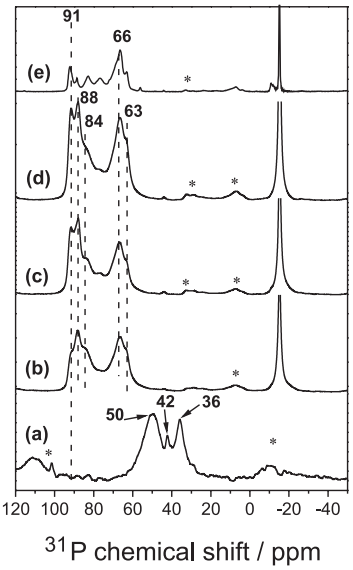

Figure 3. ^{31}P NMR spectra of TMPO adsorbed on (a) CeO_2; (b) 15HPW/CeO_2; (c) 20HPW/CeO_2; (d) 25HPW/CeO_2; (e) pristine HPW. Asterisks represent spinning sidebands.

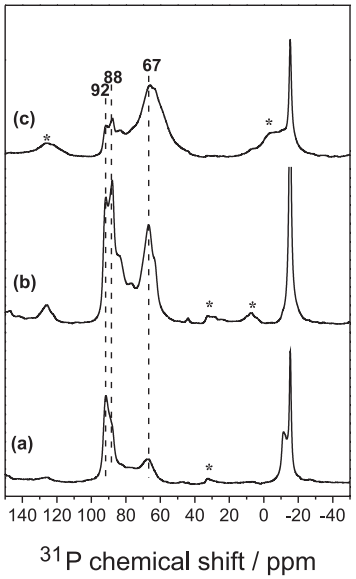

Figure 4. ^{31}P NMR spectra of TMPO adsorbed on (a) 20HPW/ZrO_2; (b) 20HPW/CeO_2; and (c) 20HPW/TiO_2. Asterisks represent spinning sidebands.

indicative that the incorporation of superacidic HPW onto the CeO_2 support tends to provoke formation of Lewis acidity. Together with the ultra-strong Brønsted acidity, a synergy effect due to Brønsted-Lewis acid sites may be inferred for the satisfying catalytic performance observed for the supported HPW/CeO_2 catalysts during oxidation of BzOH (*vide infra*).

Oxidation of benzyl alcohol to benzaldehyde

Table 2 summarizes the catalytic performances of various catalysts during oxidation of BzOH. The CeO_2 support, which possesses the weakest acidity, exhibited null activity for oxidation of BzOH. Upon incorporation of HPW onto CeO_2, a significant enhancement in catalytic activity was observed. The 15HPW/CeO_2 catalyst with HPW loading of 15 wt.% showed satisfactory BzOH conversion and BzH product yield of 77.9 and 76.0%, respectively. Upon increasing the HPW loading to 20 wt.%, notable increases in both BzOH conversion (94.0%) and BzH yield (92.3%) with excellent selectivity (98.2%) were observed. However, further increase in HPW loading to 25 wt.% led to inferior performance, the BzOH conversion and BzH yield decreased to 93.2 and 88.4%, respectively. The effect of support on BzOH oxidation were also investigated, and the results obtained from 20 wt.% HPW on ZrO_2, TiO_2 and CeTiO supports are also depicted in Table 2. Even though CeTiO, TiO_2 and ZrO_2 were found to have a larger surface area (94, 53 and 33 $m^2\,g^{-1}$, respectively) than CeO_2 (8.1 $m^2\,g^{-1}$), it is obvious that the 20HPW/CeO_2 catalyst still outperformed its counterparts for oxidation of BzOH.

The satisfying catalytic performance observed for the 20HPW/CeO_2 catalyst during oxidation of BzOH with H_2O_2 may be correlated to its acid properties, as evidenced by results obtained from ^{31}P MAS NMR of adsorbed TMPO (Figures 3 and 4) discussed above. Clearly, the presence of excessive amount of ultra-strong acidity is detrimental for oxidation of alcohol. As such, the satisfying catalytic

Table 2. Comparisons of catalytic performances over various catalysts during oxidation of benzyl alcohol[a]

Catalyst	BzOH conversion / %	BzH selectivity / %	BzH yield / %
CeO_2	nil	nil	nil
15HPW/CeO_2	77.9	97.6	76.0
20HPW/CeO_2	94.0	98.2	92.3
25HPW/CeO_2	93.2	94.7	88.4
20HPW/TiO_2	84.0	96.6	81.2
20HPW/ZrO_2	90.8	91.7	83.3
20HPW/CeTiO[b]	89.3	93.2	83.2

[a]Reactions were performed under the conditions: BzOH/H_2O_2, 1:2 (mol mol^{-1}); amount of catalyst, 0.8 g; reaction time, 4 h; amount of water, 20 mL; temperature, 110 °C; [b]CeTiO was prepared by sol-gel method.

activity observed for the 20HPW/CeO_2 catalyst may be attributed to the presence of desirable amount of strong Brønsted and Lewis acid sites. In other word, it is due to a synergetic effect of Brønsted-Lewis acid sites. Since the 20HPW/CeO_2 catalyst exhibited the best catalytic performance for oxidation of BzOH to BzH, it was exploited for the subsequent process variable optimization and kinetic studies.

Effects of reaction parameters on oxidation of benzyl alcohol

The effects of experimental parameters such as amount of catalyst, reaction time, temperature, BzOH/H_2O_2 molar ratio, and amount of water on catalytic performances during the oxidation reaction over the 20HPW/CeO_2 catalyst were studied. This is done by varying a target parameter while keeping the others fixed, as shown Figure 5. Both BzOH conversion and BzH yield increases with increasing catalyst amount (Figure 5a), reaching a plateau at ca. 0.8 g with a conversion and product yield of 94.0 and 92.3%, respectively. It is expected that more amount of catalyst in the reaction system warrants more available active moieties for catalyzing the reaction. Nevertheless, upon reacting a desirable amount of active moieties required for oxidation of BzOH, further increase in catalyst amount is redundant. Likewise, an optimal reaction time of 4 h (Figure 5b), reaction temperature of 110 °C (Figure 5c), BzOH/H_2O_2 ratio of 1:2 (Figure 5d), and amount of water of 20 mL (Figure 5e) may also be inferred. It is anticipated that reaction carried out over extended period of time and elevated temperatures may provoke occurrence of undesirable side reactions. Moreover, a desirable excessive amounts of H_2O_2 and water is favorable for driving the equilibrium towards formation of BzH, whilst an immense amount of H_2O_2 tends to dilute the reaction system, which is unfavorable for BzH selectivity and yield. The presence

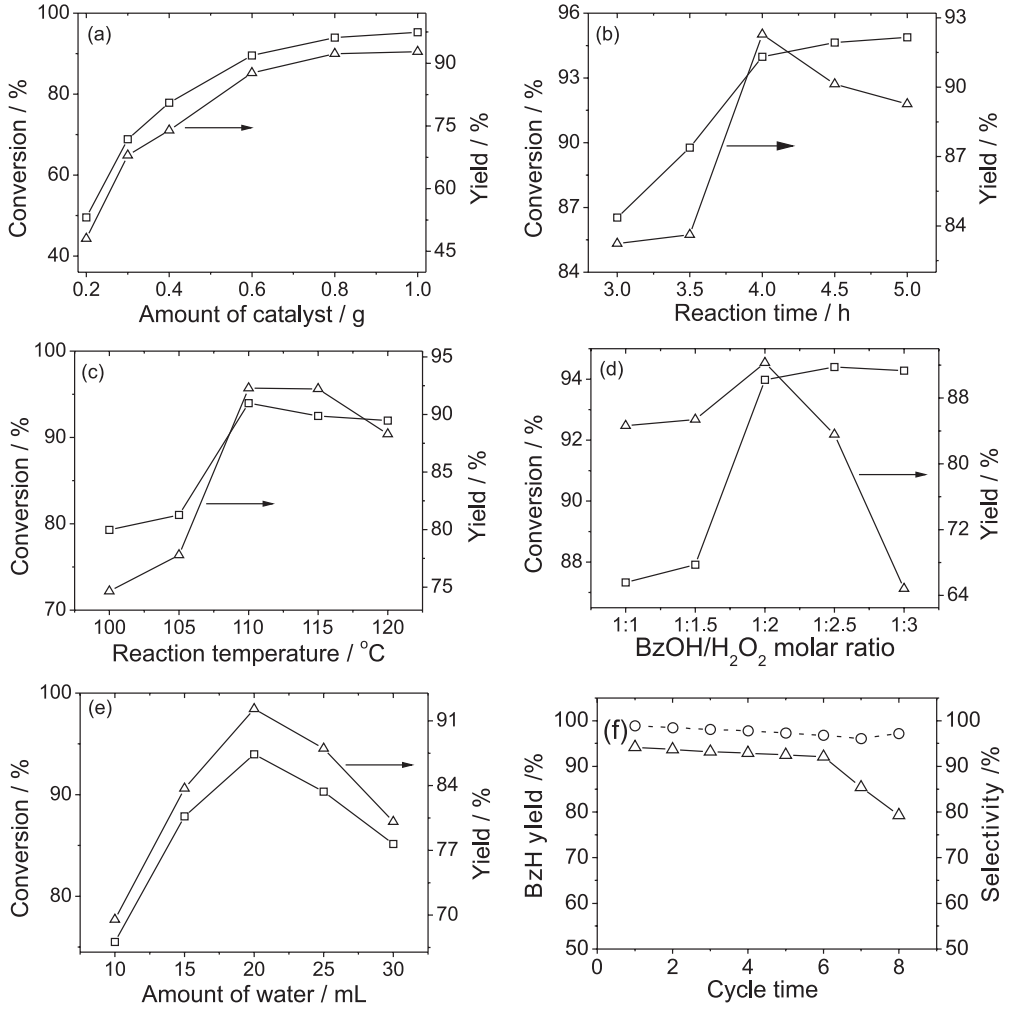

Figure 5. Effects of (a) amount of catalyst; (b) reaction time; (c) reaction temperature; (d) benzyl alcohol (BzOH) to hydrogen peroxide (H_2O_2) molar ratio; and (e) amount of water on conversion (□) and benzaldehyde yield (△) during oxidation of BzOH with H_2O_2 over the 20HPW/CeO_2 catalyst; (f) recyclability test. Unless otherwise specified, all reactions were performed under the typical conditions: amount of catalyst, 0.8 g; BzOH/H_2O_2, 1:1.2 (mol mol^{-1}); reaction time, 4.0 h; amount of water, 20.0 mL; temperature, 110 °C.

of water tends to form special droplets in the heterogeneous reaction system to favor adsorption and/or activation of oxidant during the oxidation reaction. Thus, it is conclusive that the best performance for efficient oxidation of BzOH with H_2O_2 over the 20HPW/CeO_2 catalyst may be obtained under the optimal experimental conditions: BzOH/H_2O_2, 1:2 (mol mol^{-1}); reaction time, 4.0 h; amount of catalyst, 0.8 g; amount of water, 20.0 mL; and reaction temperature, 110 °C. As a result, a maximum BzOH conversion of 94.0% and a BzH selectivity and yield of 98.2 and 92.3%, respectively, may be achieved.

RSM and ANOVA studies

A factorial analysis by analysis of variance (ANOVA) and response surface methodology (RSM) were utilized to investigate the interactive effects between experimental variables and to optimize process variables. Accordingly, the product yields (Y) predicted by multiple regression analysis may be predicted by means of a quadratic model:

$$Y = 92.28 + 6.17x_1 + 2.13x_2 + 2.79x_3 + 1.99x_4 - 5.70x_1^2 - 3.41x_2^2 - 2.00x_3^2 - 2.58x_4^2 - 1.33x_1x_2 - 3.15x_1x_3 + 0.19x_1x_4 - 2.34x_2x_3 - 2.49x_2x_4 + 0.22x_3x_4 \quad (5)$$

where x_1, x_2, x_3, and x_4 represent the coded values of the four process variables defined in Table 1, and the results are summarized in Table 3.

By fitting the experimental results with those predicted by RSM, the reliability of the fitting and validity of the proposed model in equation 5 may be assessed. As depicted in Table 4, a coefficient of determination (R^2) value of 0.9811 was achieved, revealing that only a minimal percentage (1.9%) of the fittings were unjustifiable by the model. Moreover, an F_{model} value of 51.87 and a lack-of-fit of 3.78 were obtained, implying the lack-of-fit is not significant relative to the pure error. These results indicate that the proposed model was adequate and the fittings between the experimental and predicted results are highly reliable.

Based on the RSM results, the correlations between process variable pairs for oxidation of BzOH with H_2O_2 over the 20HPW/CeO_2 catalyst may further be clarified by the contour plots and three-dimensional (3D) response surface plots shown in Figures S1 and S2 of the Supplementary Information, respectively. It was found that the correlations between catalyst loading (x_1) and BzOH/H_2O_2 molar ratio (x_2), and that of reaction time (x_3) and water amount (x_4) on BzH yield were not significant, as evidenced by the nearly circular contour plots in Figures S1a and S1f. On the other hand, the elliptical shape of the contour plots in Figures S1d and S1e revealed that correlations between x_2 (BzOH/H_2O_2 molar ratio) and x_3 (reaction time) and x_4 (water amount) were more significant. Moreover, it is obvious that the most significant effect on BzH yield arose from interactions between amount of catalyst (x_1) and reaction time (x_3), as shown in Figures S1b and S2b (Supplementary Information). The above observations are consistent with the ANOVA results depicted in Table 4 and coincide with the smaller coefficient observed for the x_1x_4 (0.19) and x_3x_4 (0.22) interactive terms in equation 5.

Based on results obtained from RSM, the optimized reaction conditions for most effective oxidation of BzOH with H_2O_2 over the 20HPW/CeO_2 catalyst may be

Table 3. List of experimental design and response values obtained for oxidation of BzOH over the 20HPW/CeO_2 catalyst

entry	Variable and level				Yield / %
	x_1	x_2	x_3	x_4	
1	−1	−1	0	0	73.00
2	1	−1	0	0	88.15
3	−1	1	0	0	80.98
4	1	1	0	0	90.82
5	0	0	−1	−1	84.55
6	0	0	1	−1	88.23
7	0	0	−1	1	86.86
8	0	0	1	1	91.41
9	−1	0	0	−1	75.38
10	1	0	0	−1	88.50
11	−1	0	0	1	80.24
12	1	0	0	1	94.13
13	0	−1	−1	0	80.17
14	0	1	−1	0	88.09
15	0	−1	1	0	91.47
16	0	1	1	0	90.03
17	−1	0	−1	0	72.34
18	1	0	−1	0	89.63
19	−1	0	1	0	84.61
20	1	0	1	0	89.31
21	0	−1	0	−1	79.08
22	0	1	0	−1	88.30
23	0	−1	0	1	88.02
24	0	1	0	1	87.29
25	0	0	0	0	91.61
26	0	0	0	0	91.70
27	0	0	0	0	93.00
28	0	0	0	0	92.11
29	0	0	0	0	93.00

Table 4. List of results obtained from ANOVA for BzH yield

Source	Sum of square	DF	Mean square	*F*	*P* > *F*	Significance
Model	1002.33	14	71.60	51.87	< 0.0001	[a]
x_1	456.21	1	456.21	330.52	< 0.0001	[a]
x_2	54.70	1	54.70	39.63	< 0.0001	[a]
x_3	93.07	1	93.07	67.43	< 0.0001	[a]
x_4	47.64	1	47.64	34.52	< 0.0001	[a]
x_1^2	210.52	1	210.52	152.52	< 0.0001	[a]
x_2^2	75.35	1	75.35	54.59	< 0.0001	[a]
x_3^2	25.84	1	25.84	18.72	0.0007	[a]
x_4^2	43.33	1	43.33	31.39	< 0.0001	[a]
x_1x_2	7.05	1	7.05	5.11	0.0403	[b]
x_1x_3	39.63	1	39.63	28.71	0.0001	[a]
x_1x_4	0.15	1	0.15	0.11	0.7480	
x_2x_3	21.90	1	21.90	15.87	0.0014	[a]
x_2x_4	24.75	1	24.75	17.93	0.0008	[a]
x_3x_4	0.19	1	0.19	0.14	0.7167	
Residual	19.32	14	1.38			
Lack-of-fit	17.47	10	1.75	3.78	0.1061	NS
Pure error	1.85	4	0.46			
Cor. total	1021.66	28				

DF: degree of freedom; NS: non-significant; [a]highly significant; [b]significant.

derived as the following: amount of catalyst (x_1) = 0.84 g, BzOH/H_2O_2 ratio (x_2) = 1:1.19 mol mol^{-1}, reaction time (x_3) = 4.43 h, and amount of water (x_4) = 22.31 mL, leading to a predicted BzH yield of 94.6%. These theoretical results are in excellent agreement with the experimental data. To further verify the validity of the predicted BzH yield, three parallel experiments were carried out independently over the 20HPW/CeO_2 catalyst using these predicted reaction variables. As a result, an experimental BzH yield of 94.2% was achieved (with BzOH conversion of 95.2% and BzH selectivity of 98.9%), in excellent agreement with the predicted yield (94.6%).

Catalyst recycling test

The durability and reusability of the 20HPW/CeO_2 catalyst for oxidation of BzOH with H_2O_2 under the simplified process conditions, *viz*. amount of catalyst = 0.84 g, BzOH/H_2O_2 molar ratio = 1:1.2 mol mol^{-1}, reaction time = 4.4 h, and amount of water = 22.3 mL, were further tested for six consecutive experimental runs. Note that, upon completion of each run, the catalyst was filtered and washed (by diethyl ether) and reused after drying under vacuum for 8 h at 70 °C. As shown in Figure 5f, the 20HPW/CeO_2 catalyst exhibited good reusability. The BzH yield and selectivity BzH decreased from ca. 94.2 and 98.9% of the initial cycle to ca. 92.1 and 96.8% of the 6th cycle, respectively. Additional FTIR measurements also revealed that the structural integrity of the 20HPW/CeO_2 catalyst remained practically unchanged for the spent catalyst obtained after six consecutive runs (Figure S3; Supplementary Information). However, the yield of BzH was decreased largely to 85.4 and 79.3% for the 7th and 8th cycle, respectively. The decrease in catalytic activity observed during cyclic tests may be attributed to the loss of HPW during the regeneration treatment; as evidenced by elemental analyses using the inductively coupled plasma (ICP) technique (ICP-OES CID spectrometer, ICAP 6500; Thermo Scientific). It was found that the overall concentration of P atom decreased from 0.21 wt.% of the fresh catalyst to 0.13 wt.% of the regenerated spent catalyst obtained after eight running cycles. In spite of this drawback, the above results clearly indicate that the 20HPW/CeO_2 catalyst is indeed robust and durable for catalytic oxidation reaction, thus, render practical industrial applications.

Kinetic study

The kinetic parameters involved during catalytic oxidation of BzOH over the 20HPW/CeO_2 catalyst were

also determined. As shown in Figure 6a, by monitoring BzOH conversion with varied initial concentrations (i.e., C_A), the corresponding value of reaction rate (r) may be obtained based on equation 2, while the reaction order of BzOH (α) may be derived by equation 3, as shown in Figure 6b. As a result, an α value of 1.73 was obtained with a satisfactory correlation coefficient (R^2) of 0.996. Likewise, by varying the initial concentrations of H_2O_2 (i.e., C_B), an H_2O_2 reaction order (β) of 0.38 with $R^2 = 0.999$ was obtained, as seen in Figure 7.

Moreover, by plotting the variations of BzOH concentration (i.e., C_A) *versus* reaction time during oxidation of BzOH over the 20HPW/CeO_2 catalyst under the optimized reaction conditions (namely, amount of catalyst = 0.84 g, BzOH/H_2O_2 = 1:1.2 mol mol^{-1}, reaction time 4.4 h, and amount of water of 22.3 mL), the rate constants at different reaction temperatures may be obtained, as shown in Figure 8a. Accordingly, based on equation 4, the Arrhenius plot of ln k *vs*. 1/T in Figure 8b may be used to derive the activation energy (Ea) of the reaction, which is 44.7 kJ mol^{-1}. Overall, the rate equation for oxidation of BzOH with H_2O_2 over the 20HPW/CeO_2 catalyst may readily be written as:

$$r = -\frac{dC_A}{dt} = e^{9.6\left(-\frac{44.7}{RT}\right)} C_A^{1.7} C_B^{0.4} \quad (6)$$

It is noteworthy that the E_a value obtained for the present catalytic system for oxidation of BzOH is much lower than that for oxidation of substituted phenethyl alcohols over the *N*-chlorinated *p*-toluenesulfonamide (*p*-TSA) salt (81.3 kJ mol^{-1})[41] and for the oxidation of furfuryl alcohol over heterogeneous nano zirconium chromate catalyst in THF (76.7 kJ mol^{-1}).[42] This indicates that the 20HPW/CeO_2 catalyst is indeed a highly effective catalyst for oxidation of benzyl alcohol to benzaldehyde.

Conclusions

Composite catalysts synthesized by incorporating the superacidic tungstophosphoric acid (HPW) on a ceria (CeO_2) support have been successfully prepared and exploited for oxidation of benzyl alcohol (BzOH) with hydrogen peroxide (H_2O_2). Among various composite catalysts examined, the catalyst of 20HPW/CeO_2 loaded with 20 wt.% of HPW was found to exhibit satisfying catalytic activity with excellent BzOH conversion (94.0%)

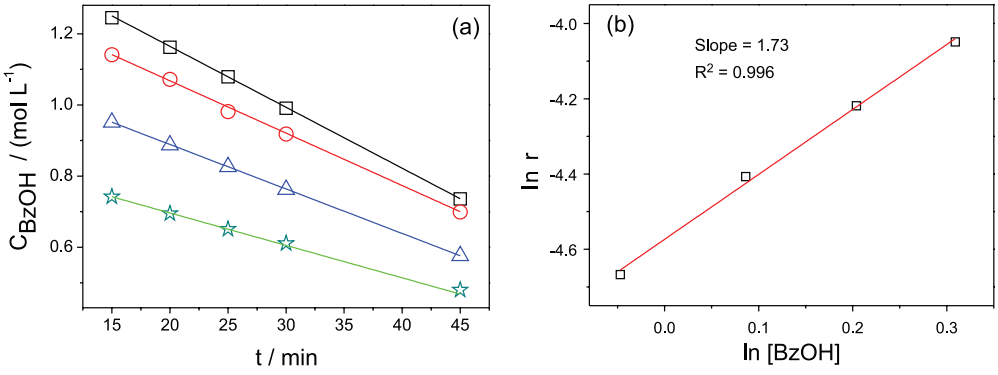

Figure 6. (a) Variations of BzOH concentration (C_A) *versus* reaction time; symbols for initial C_A values: 1.36 (□), 1.23 (○), 1.09 (△), and 0.95 mol L^{-1} (☆); (b) log-log plot of initial oxidation rate (r) *vs*. initial C_A. Reaction conditions: temperature, 110 °C; initial H_2O_2 concentration, 2.73 mol L^{-1}; initial BzH concentration, 0 mol L^{-1}; amount of catalyst, 22.22 g L^{-1}.

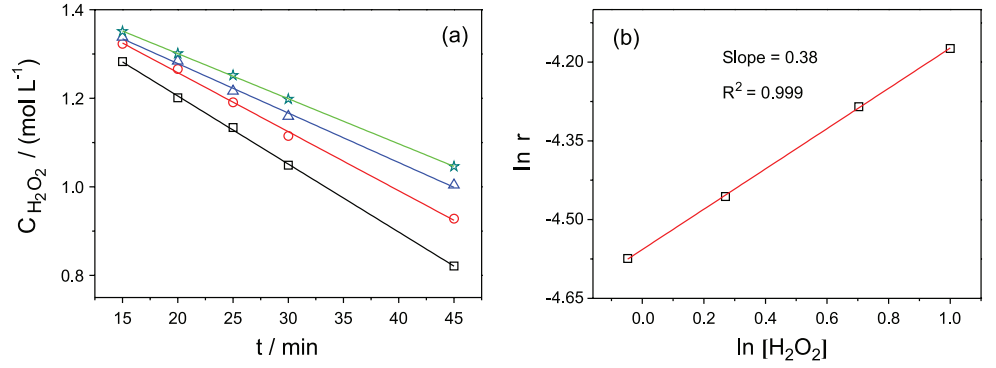

Figure 7. (a) Variations of H_2O_2 concentration (C_B) *versus* reaction time; symbols for initial C_B values: 2.72 (□), 2.02 (○), 1.31 (△), and 0.95 mol L^{-1} (☆); (b) log-log plot of initial oxidation rate *vs*. initial C_B. Reaction conditions: temperature, 110 °C; initial BzOH concentration, 1.36 mol L^{-1}; initial H_2O_2 concentration, 0 mol L^{-1}; amount of catalyst, 22.22 g L^{-1}.

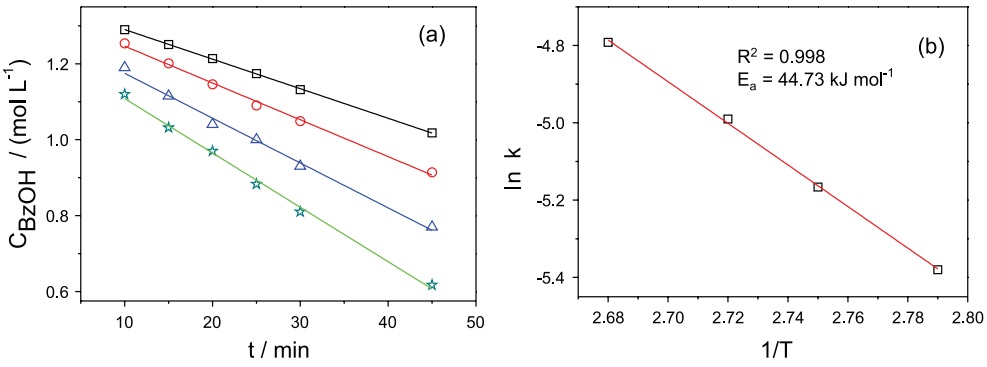

Figure 8. (a) Variations of BzOH concentration *versus* reaction time under different reaction temperatures: 95 (□), 100 (○), 105 (△), and 110 °C (☆); (b) the corresponding Arrhenius plot; reaction conditions: initial BzOH concentration, 1.36 mol L^{-1}; initial H_2O_2 concentration, 2.73 mol L^{-1}; amount of catalyst, 22.22 g L^{-1}.

and BzH yield (92.3%) and selectivity (98.2%). The satisfying catalytic activity observed for the composite catalyst is attributed to the strong acidity and Brønsted-Lewis acid synergy effect. Process optimization based on RSM rendered prediction of optimized reaction parameters, namely, amount of catalyst 0.84 g, BzOH/H_2O_2 ratio 1:2 mol mol^{-1}, reaction time 4.4 h, and amount of water 22.3 mL at a reaction temperature of 110 °C. Accordingly, the value of BzOH conversion, BzH yield, and BzH selectivity of 95.2, 94.2, and 98.9%, respectively, were derived, in good agreement with the experimental results. Such supported HPW/CeO_2 catalysts, which are cost-effective and may be easily prepared in mass quantity, also exhibit excellent activity, durability, and recyclability, showing prospective applications for large-scale oxidation of alcohols.

Supplementary Information

Supplementary data associated with this article can be found, in the online version, at http://jbcs.sbq.org.br as PDF file.

Acknowledgments

The supports of this work by the Project of Science and Technology Department of Zhejiang Province (No. 2016C31016), the Program for Zhejiang Leading Team of S & T Innovation (No. 2013TD07), and the Ministry of Science and Technology, Taiwan (NSC 104-2113-M-001-019) are gratefully acknowledged.

References

1. Xu, C.; Zhang, C.; Li, H.; Zhao, X.; Song, L.; Li, X.; *Catal. Surv. Asia* **2016**, *20*, 13.
2. Du, Y. Y.; Wang, Q.; Liang, X.; He, Y. F.; Feng, J. T.; Li, D. Q.; *J. Catal.* **2015**, *331*, 154.
3. Choudhary, V. R.; Jha, R.; Jana, P.; *Green Chem.* **2007**, *9*, 267.
4. Friedrich, H. B.; *Platinum Met. Rev.* **1999**, *43*, 94.
5. Enache, D. I.; Edwards, J. K.; Landon, P.; Solsona-Espriu, B.; Carley, A. F.; Herzing, A. A.; Watanabe, M.; Kiely, C. J.; Knight, D. W.; Hutchings, G. J.; *Science* **2006**, *311*, 362.
6. Cortés Corberán, V.; González-Pérez, M. E.; Martínez-González, S.; Gómez-Avilés, A.; *Appl. Catal., A* **2014**, *474*, 211.
7. Liu, C. H.; Lin, C. Y.; Chen, J. L.; Lu, K. T.; Lee, J. F.; Chen, J. M.; *J. Catal.* **2017**, *350*, 21.
8. Ahmad, J. U.; Räisänen, M. T.; Leskelä, M.; Repo, T.; *Appl. Catal., A* **2009**, *371*, 17.
9. Sudarsanam, P.; Mallesham, B.; Naga Durgasri, D.; Reddy, B. M.; *J. Ind. Eng. Chem.* **2014**, *20*, 3115.
10. Yu, X.; Huo, Y.; Yang, J.; Chang, S.; Ma, Y.; Huang, W.; *Appl. Surf. Sci.* **2013**, *280*, 450.
11. Kim, H. J.; Jeon, Y. K.; Park, J.; Shul, Y. G.; *J. Mol. Catal. A: Chem.* **2013**, *378*, 232.
12. Farsani, M. R.; Jalilian, F.; Yadollahi, B.; Rudbari, H. A.; *Polyhedron* **2014**, *76*, 102.
13. Tokarz-Sobieraj, R.; Grybos, R.; Filek, U.; Micek-Ilnicka, A.; Niemiec, P.; Kirpsza, A.; Witko, M.; *Catal. Today* **2015**, *257*, 72.
14. Leng, Y.; Zhao, P.; Zhang, M.; Wang, J.; *J. Mol. Catal. A: Chem.* **2012**, *358*, 67.
15. Pamin, K.; Prończuk, M.; Basąg, S.; Kubiak, W.; Sojka, Z.; Połtowicz, J.; *Inorg. Chem. Commun.* **2015**, *59*, 13.
16. Zhao, W.; Zhang, Y.; Ma, B.; Ding, Y.; Qiu, W.; *Catal. Commun.* **2010**, *11*, 527.
17. Farsani, M. R.; Yadollahi, B.; *J. Mol. Catal. A: Chem.* **2014**, *392*, 8.
18. Choi, J. H.; Kang, T. H.; Song, J. H.; Bang, Y.; Song, I. K.; *Catal. Commun.* **2014**, *43*, 155.
19. Dong, D. R.; Choi, J. H.; Park, S.; Song, I. K.; *Appl. Catal., A* **2011**, *394*, 201.
20. Wang, S. S.; Zhang, J.; Zhou, C. L.; Vo-Thanh, G.; Liu, Y.; *Catal. Commun.* **2012**, *28*, 152.

21. Pathan, S.; Patel, A.; *Appl. Catal., A* **2013**, *459*, 59.
22. Madhusudhan Rao, P.; Wolfson, A.; Kababya, S.; Vega, S.; Landau, M. V.; *J. Catal.* **2005**, *232*, 210.
23. Chen, L. J.; Feng, T.; Wang, P. F.; Chen, Z. W.; Yana, R. Q.; Liao, B.; Xiang, Y. J.; *Appl. Catal., A* **2016**, *523*, 304.
24. Ghanbari-Siahkali, A.; Philippou, A.; Dwyer, J.; Anderson, M. W.; *Appl. Catal., A* **2000**, *192*, 57.
25. Izumi, Y.; Urabe, K.; *Chem. Lett.* **1981**, *10*, 663.
26. Hu, C.; He, Q.; Zhang, Y.; Liu, Y.; Zhang, Y.; Tang, T.; Zhang, J.; Wang, E.; *Chem. Commun.* **1996**, *2*, 121.
27. Vlaic, G.; Di Monte, R.; Fornasiero, P.; Fonda, E.; Kaspar, J.; Graziani, M.; *J. Catal.* **1999**, *182*, 378.
28. Gokhan, E.; Demet, O.; Birgul, Z. K.; *Catal. Commun.* **2017**, *89*, 56.
29. Reddy, B. M.; Khan, A.; *Catal. Surv. Asia* **2005**, *9*, 155.
30. Narasimharao, K.; Ali, T. T.; *Catal. Lett.* **2013**, *143*, 1074.
31. Zhang, H.; Xie, Y.; Sun, Z.; Tao, R.; Huang, C.; Zhao, Y.; Liu, Z.; *Langmuir* **2011**, *27*, 1152.
32. Abad, A.; Concepcion, P.; Corma, A.; Garcfa, H.; *Angew. Chem., Int. Ed.* **2005**, *44*, 4066.
33. Ragupathi, C.; Judith Vijaya, J.; Narayanan, S.; Jesudoss, S. K.; John Kennedy, L.; *Ceram. Int.* **2015**, *41*, 2069.
34. Zheng, A.; Huang, S. J.; Liu, S. B.; Deng, F.; *Phys. Chem. Chem. Phys.* **2011**, *13*, 14889.
35. Zheng, A.; Li, S.; Liu, S. B.; Deng, F.; *Acc. Chem. Res.* **2016**, *49*, 655.
36. Zheng, A.; Huang, S. J.; Chen, W. H.; Wu, P. H.; Zhang, H.; Lee, H. K.; De Ménorval, L. C.; Deng, F.; Liu, S. B.; *J. Phys. Chem. A* **2008**, *112*, 7349.
37. Zheng, A.; Zhang, H.; Lu, X.; Liu, S. B.; Deng, F.; *J. Phys. Chem. B* **2008**, *112*, 4496.
38. Essayem, N.; Gayraud, A. P. Y.; Vedrine, J. C.; Taarit, Y. B.; *J. Catal.* **2001**, *197*, 273.
39. Huang, S. J.; Yang, C. Y.; Zheng, A.; Feng, N.; Yu, N.; Wu, P. H.; Chang, Y. C.; Lin, Y. C.; Deng, F.; Liu, S. B.; *Chem. Asian J.* **2011**, *6*, 137.
40. Khder, A. E. R. S.; Hassan, H. M. A.; El-Shal, M. S.; *Appl. Catal., A* **2012**, *411-412*, 77.
41. Ramachandra, H.; Rangappa, K. S.; Mahadevappa, D. S.; MadeGowda, N. M.; *Monatsh. Chem.* **1996**, *127*, 241.
42. Setareh, S.; Nooredin, G.; *Monatsh. Chem.* **2016**, *147*, 1531.

Submitted: January 25, 2017
Published online: June 26, 2017